Novel Carbohydrate-substituted Indazole Derivatives Targeting SGLT1 Enhance the Efficacy of Receptor Tyrosine Kinase Inhibitors in Cancer Therapy

Zhongjie Sun[1,2,*], Hailong Qi[1,2,*]

[1]Newish Biological R&D Center, Wuxi, China

[2]These authors contributed equally: Hailong Qi, Zhongjie Sun

*Correspondence: szj@newishes.com; qihailong3@newishes.com.

Abstract

Receptor tyrosine kinase (RTK) inhibitors have demonstrated significant efficacy in treating malignant tumors. However, the development of drug resistance and limited efficacy in RTK inhibitor-insensitive patients pose challenges to their clinical application. To enhance the efficacy for RTK inhibitors-insensitive patients and overcome the resistance, beyond developing new RTK inhibitors, combination therapy has emerged as a promising approach. In this study, we discovered a novel compound, **071**, featuring an indazole core flanked by a carbohydrate moiety and two phenyl groups, which exhibits synergistic anti-tumor activity when combined with various RTK inhibitor. Several series of **071** analogues were synthesized through structure modification and evaluated the synergistic anti-tumor effects and the metabolic stability. Compound **10d-02** emerged as notably more potent in synergistic anti-tumor activity and demonstrated greater stability than compound **071**. Notably, the combination of compound **10d-02** and multiple RTK inhibitors significantly enhanced in vivo efficacy in both RTK inhibitor-sensitive and -insensitive tumor xenograft models without evident toxicity. Furthermore, compound **10d-02** exhibited an excellent pharmacokinetic profile with nearly 100% oral bioavailability. Using click chemistry technology combined with mass spectrometry analysis, we identified SGLT1 as a potential target for **10d-02**. SGLT1 has been previously proven to bind and stabilize EGFR, and we further discovered that SGLT1 also binds and stabilizes VEGFR2/3. While compound **10d-02** could partially block the interaction between SGLT1 and EGFR/VEGFRs, leading to the instability and degradation of EGFR and VEGFRs, potentially elucidating the mechanism of its synergistic effect with RTK inhibitors. Thus, compound **10d-02** holds substantial promise for use in combination therapies with RTK inhibitors in tumor clinical treatment.

Key words: Indazole Derivatives, SGLT1, Combination therapy, RTK inhibitors, Cancer treatment.

Introduction

A variety of receptor tyrosine kinase (RTK)-targeted drugs are currently employed in cancer therapy [1]. RTKs, including the epidermal growth factor receptor (EGFR) family (EGFR, HER2, HER3, HER4) [2], vascular endothelial growth factor receptor (VEGFR) family (VEGFR1, VEGFR2, VEGFR3) [3], insulin-like growth factor receptor (IGF1R)[4], and fibroblast growth factor receptor (FGFR)[5], activate downstream signaling pathways such as phosphatidylinositol-3-kinase (PI3K)/ protein kinase B (AKT) pathway, Ras/Raf mitogen activated protein kinase (MAPK) pathway, and the Janus kinase (JAK)/signal transducer and activator of transcription (STAT) pathway upon autophosphorylation. The aberrant expression or mutations in RTKs lead to the inappropriate activation of these signaling pathways, consequently driving the excessive proliferation of cancer cells [6]. RTK inhibitors function by blocking these signaling pathways, thereby offering a therapeutic approach for the treatment of cancer. Among these RTK inhibitors, EGFR inhibitors are extensively studied and have shown remarkable efficacy in blocking the phosphorylation-mediated signaling pathways activation in various malignancies [7], such as Osimertinib, a third-generation EGFR inhibitor, used for treating non-small-cell lung cancer (NSCLC) patients harboring the T790M mutation [8]. In addition, the VEGFR inhibitors are also widely used in the treatment of various tumors by suppressing tumor-induced angiogenesis[9], such as, Apatinib as a selective VEGFR-2 inhibitor was approved in China to treat advanced or metastatic gastric cancer [10]. Despite their benefits, the clinical application of these inhibitors is often limited by drug resistance, reduced efficacy, and potential toxicity in most patients [11,12]. Therefore, developing new strategies to improve clinical outcomes, overcome resistance and minimize the toxic effects are required.

The combination therapy of anti-cancer drugs provides a promising method to improve clinical outcomes and overcome resistance [13]. The combination therapy primarily targets bypass pathways, including the suppression of parallel pathways, inhibition of downstream pathways, or integration with other drugs that possess potential anti-tumor

properties [14]. For instance, a synergistic effect has been observed between the FGFR inhibitor Erdafitinib and the PI3K inhibitor pictilisib in a model of FGFR-driven urothelial cancer with activating PIK3CA mutations [15]. Similarly, the combination of the EGFR inhibitor Osimertinib with the MET inhibitor Savolitinib has been shown to restore Osimertinib sensitivity in cases of MET-driven resistance [16]. Additionally, combining VEGFR inhibitors with immune checkpoint inhibitors has significantly improved outcomes in patients with renal cell carcinoma compared to monotherapy with VEGFR inhibitors alone [17].

In this study, we conducted a random screening of our in-house compound library to evaluate the potency and efficacy of combination with RTK inhibitors in tumor cells. This screening led to the identification of a novel compound, **071** (Fig. **1A**), characterized by an indazole core flanked by a carbohydrate moiety and two phenyl groups, which demonstrated synergistic anti-tumor activity when combined with RTK inhibitors, including Apatinib, Osimertinib, Gefitinib. To further understand the structure-activity relationship and enhance the combination effect, we performed the structure modification of compound **071** to design and synthesis kinds of target compounds. This paper details the synthesis, structure-activity relationship, pharmacokinetic properties, in vivo anti-tumor efficacy of combination with different RTK inhibitors and explore their possible mechanism of action.

Results and discussion

Compound 071 exhibits synergistic anti-tumor effects when combined with various RTK inhibitors.

We utilized the gastric cancer cell line HGC-27 cells and NSCLC cell line H1975 to screen our in-house compound library, assessing the activity combination with three classical RTK inhibitors. Our findings revealed that the compound **071** significantly enhanced the cytotoxicity of Apatinib, which is a is a VEGFR inhibitor approved for the treatment of gastric cancer. Additionally, combination with compound **071** improved the activity of the third generation EGFR inhibitor Osimertinib on H1975 cell line which contains EGFR T790M mutation and is sensitive to Osimertinib treatment (Fig. 1B and1C). These results indicated that combinations of compound **071** with RTK inhibitors frequently yield synergistic anti-tumor effect.

Due to the T790M mutation, the H1975 cell line is insensitive to the treatment with first-generation EGFR inhibitor Gefitinib. We next tested whether compound **071** could enhance the activity of Gefitinib on H1975 cells. We assessed the survival curves of H1975 cell line treated with various concentrations of Gefitinib, both alone and in combination with 15 μM of Compound **071** (Fig. 1D). The cytotoxicity was evaluated via the determination of the half maximal inhibitory concentration (IC_{50}) using the MTT assay. The results showed that IC_{50} values of Gefitinib for H1975 cells was 201μM, indicating a resistance to Gefitinib in H1975 cells. Notably, the combination of Compound **071** and Gefitinib enhanced the toxicity of Gefitinib in H1975 cell lines which reduced the IC_{50} of Gefitinib from 201 μM to 3.72 μM in H1975 cells. We also tested the cytotoxicity of compound **071** and Gefitinib on another NSCLC cell line A549 harboring wild-type EGFR. A549 cells are also insensitive to Gefitinib treatment. Consistent with the results observed in the H1975 cell line, the combination of compound **071** reduced the IC_{50} of Gefitinib from 12.25 μM to 1.29 μM (Fig. 1E). These results demonstrated an enhanced cytotoxicity of various types of RTK inhibitors

when combined with compound **071**.

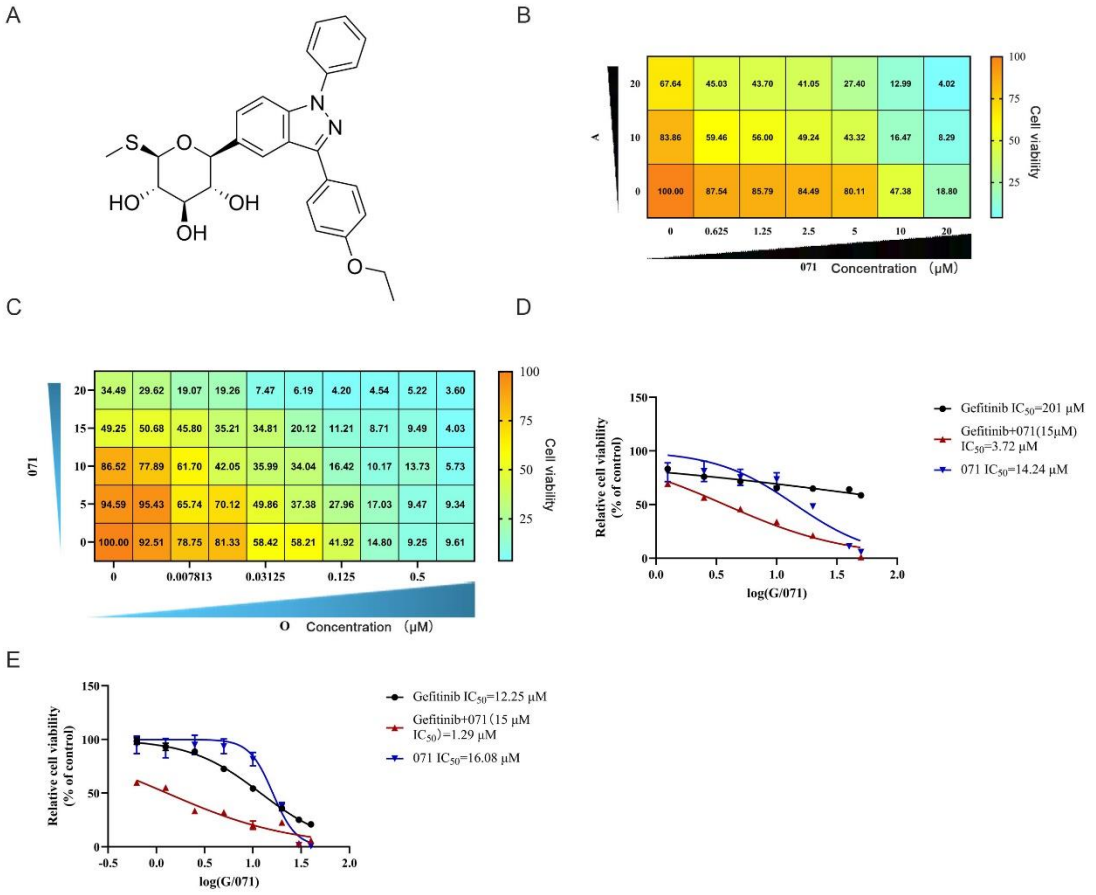

Figure 1. Compound **071** plays synergistic anti-tumor roles with different RTK inhibitors. (A) Stucture of compound **071**. (B) The cell viability of HGC-27 cells treated with varying concentrations of **071** in combination with Apatinib (A, 0, 10, 20 μM). (C) The cell viability of H1975 cells treated with varying concentrations of Osimertinib in combination with **071** (**071**, 0, 5, 10, 15, 20 μM). (D) and (E) Survival curves of H1975 or A549 cells treated with varying concentrations of Gefitinib in combination with **071** (15 μM) or Gefitinib and **071** alone.

Chemistry

To further enhance the combination effect and explore the structure-activity relationship (SAR), the structural modifications on compound **071** was performed. Our initial focus was on investigating the influence of N-linked group in indazole scaffold of compound

071 on the activity of combination to design the synthetic routes. To simplify the synthetic steps, sotagliflozin (**1**) was utilized as the starting material (Fig. 2A). Initially, sotagliflozin was acetylated using acetic anhydride (Ac_2O) in the presence of pyridine and 4-dimethylaminopyridine (DMAP), yielding compound **2**. Subsequently, compound **2** underwent oxidation with DDQ in a solvent mixture of CH_2Cl_2, 1,4-dioxane and H_2O, which provided the key intermediate **3**. The acetyl group of the intermediate **3** was hydrolyzed with LiOH in methanol (MeOH), resulting in compound **4**. The reaction of compound **4** and various substituted phenylhydrazine **5** under the catalyst of H_2SO_4 yielded the corresponding hydrazones **6**. Finally, the treatment of compound **6** with dimethylglycine, Cs_2CO_3 and CuI in dimethylacetamide (DMA) afforded target compounds **10** (Fig. 2A, Method **1**). Alternatively, the target compounds were prepared using a second method (Fig. 2A, Method **2**). This approach involved the condensation of the key intermediate **3** with 4-methylbenzenesulfonohydrazide ($TsNHNH_2$) in the presence of H_2SO_4 yielding the compound **7**. The acetyl group of compound **7** was subsequently hydrolyzed by LiOH in MeOH to produce the compound **8**. Treatment of compound **8** with dimethylglycine, Cs_2CO_3 and CuI in DMA afforded compound **9**. Ultimately, the reaction of compound **9** with various halogenated hydrocarbon under alkaline conditions afforded the corresponding target compound **10** (Fig. 2A, Method **2**). In general, the method **2** is superior to the method **1** as it involves cheaper chemicals and requires fewer steps for synthesizing multiple compounds.

To further investigate the effect of C-linked aryl groups in the indazole scaffold of compound **071** on combination activity, we also synthesized analogues containing different aromatic rings instead of the 4-ethoxy phenyl group of compound **071**. The synthetic route is illustrated in Fig. **2B**. The synthetic route for compound **11** is detailed in Scheme S1 in the supplemental data, and the commercially available compound **12**, catalyzed by n-BuLi in a mixed solvent of dry THF and toluene, produced compound **13**. Compound **14** was obtained by reducing carbonyl group of compound **13** in the presence of $NaBH_4$ and $CeCl_3$ in MeOH. Subsequently, rearrangement of compound **14** in AcOH and H_2O at 100°C yielded compound **15**. The compound **15** then was

acetylated using Ac_2O in presence of pyridine and DMAP in acetonitrile (ACN) to produce compound **16**. Next compound **16** reacted with thiourea and TMSOTF in dry dioxane at 90°C under a nitrogen atmosphere to give an intermediate, which then reacted with CH_3I in the catalysis of DIEA to obtain the compound **17**. The acetyl group in indazole ring of compound **17** was hydrolyzed using Na_2CO_3 in MeOH to obtain compound **18**. Iodination of compound **18** was conducted using NIS in DMF to provide the key intermediate **19**. The Suzuki coupling reaction of the intermediate **19** with substituted benzoic acid or borate (**20a-20h**), catalyzed by the catalysis of $Pd(PPh_3)_2Cl_2$ and Na_2CO_3 in the mixed solvent of THF and H_2O, yielded the corresponding compound **21a-21h**. Subsequently, compound **21a-21h** reacted with iodobenzene in the presence of CuI, K_2CO_3 and N^1,N^2-dimethylcyclohexane-1,2-diamine at 110°C in DMF to provide compound **22a-22h**. Finally, the acetyl groups of compound **22a-22h** were hydrolyzed using LiOH in the mixed solvent of MeOH and H_2O to obtain the target compound **23a-23g**. In addition, the target compound **23i** and **23j** were synthesized via alternative synthetic routes, as illustrated in Scheme **S2** and **S3** in supplemental data. Some of the substituted borates (**20g** and **20h**), which are not commercially available, were synthesized as shown in the Scheme S**4** in supplemental data. The stuctures of target compounds are shown in Table 1 and 2.

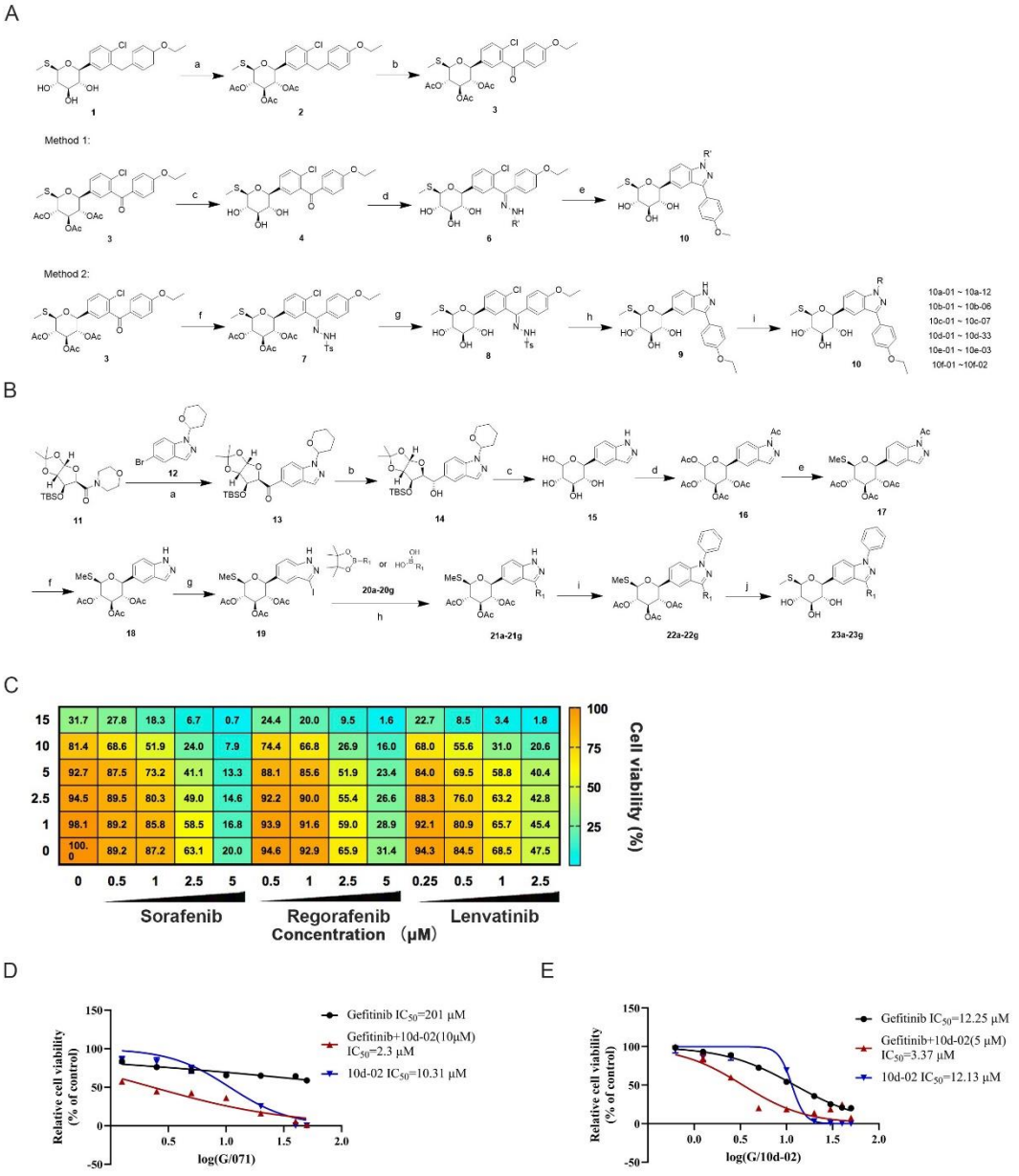

Figure 2. Structural optimization of compound **071.** (A) Scheme of synthesis of target compounds of N-linked different groups in indazole scaffold of **071**. Reagents and conditions: (a) Ac_2O, pyridine, DMAP, CH_3CN, rt; (b) DDQ, CH_2Cl_2/1,4-dioxane/H_2O, 0°C-rt; (c) LiOH, MeOH, rt; (d) NH_2NHR' (**5**), H_2SO_4, EtOH/H_2O, 100°C; (e) dimethylglycine, CuI, Cs_2CO_3, DMA, 130°C; (f) H_2SO_4, $TsNHNH_2$, EtOH, 80°C; (g) LiOH, MeOH, rt; (h) dimethylglycine, CuI, Cs_2CO_3, DMA, 130°C; (i) RX, CuI, K_2CO_3, N^1,N^2-dimethylcyclohexane-1,2-diamine, DMF, 110°C. (B) Scheme **of s**ynthesis of target compounds with C-linked different groups in indazole scaffold of **071**. Reagents

and conditions: (a) n-BuLi, THF/toluene, -65°C; (b) $NaBH_4$, $CeCl_3$, MeOH, 0°C-rt; (c) AcOH/H_2O, 100°C; (d) Ac_2O, pyridine, DMAP, ACN, rt; (e) thiourea, TMSOTf, dioxane, 90°C; CH_3I, DIEA, rt; (f) Na_2CO_3, MeOH, rt; (g) NIS, DMF, rt; (h) $Pd(dppf)_2Cl_2$, Na_2CO_3, THF/H_2O, 100°C; (i) iodobenzene, CuI, K_2CO_3, N^1,N^2-dimethylcyclohexane-1,2-diamine, DMF, 110°C. (j) LiOH, MeOH, rt. (C) The cell viability of JHH-7 cells treated with varying concentrations of Sorafenib, Regorafenib and Lenvatinib in combination with **10d-02** (**10d-02**, 0, 1, 2.5, 5, 10, 15, μM). (D) and (E) Survival curves of H1975 or A549 cells treated with varying concentrations of Gefitinib in combination with **10d-02** (5 μM) or Gefitinib and **10d-02** alone.

Table 1. The stuctures of target compounds of C-linked different group in indazole scaffold of compound **071**.

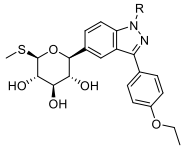

Compd.	R	Compd.	R	Compd.	R	Compd.	R	Compd.	R
Apatinib	-	10a-12		10c-07		10d-13	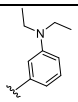	10d-26	
071		10b-01		10d-01		10d-14		10d-27	
10a-01	H	10b-02		10d-02		10d-15		10d-28	
10a-02	CH_3	10b-03		10d-03		10d-16		10d-29	
10a-03	CH_2CH_2F	10b-04		10d-04		10d-17		10d-30	
10a-04		10b-05		10d-05		10d-18		10d-31	
10a-05		10b-06		10d-06		10d-19		10d-32	
10a-06		10c-01		10d-07		10d-20	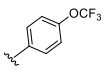	10d-33	

10a-07		10c-02		10d-08		10d-21	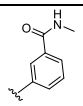	10e-01	
10a-08		10c-03		10d-09	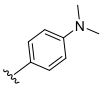	10d-22	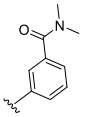	10e-02	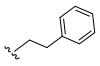
10a-09		10c-04		10d-10		10d-23		10e-03	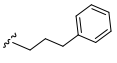
10a-10		10c-05		10d-11	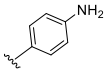	10d-24		10f-01	
10a-11		10c-06		10d-12		10d-25		10f-02	

Table 2. The stuctures of target compounds of N-linked different group in indazole scaffold of compound **071**.

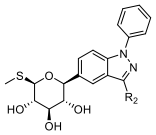

Compd.	R_2	Compd.	R_2	Compd.	R_2
23a		23d		23g	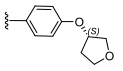
23b		23e	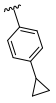	23h	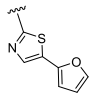
23c		23f		23i	

In vitro combination effects of target compounds with Apatinib

After synthesizing these compounds, we assessed the in vitro cytotoxicity of the target compounds both alone and in combination with 10 μM Apatinib using the human tumor cell line HGC-27. The results were presented in Table S**1**-S**4** and **S7-S9**. Substituting the N-linked phenyl group of compound **071** with hydrogen (**10a-01**), various substituted alkyl groups (**10a-02**~**10a-04**), or saturated aliphatic ring (**10a-05**~**10a-12**) resulted in a loss or reduction of cytotoxicity for both target compounds alone and their combination with Apatinib (Table S**1**).

When the N-linked phenyl group of compound **071** was replaced with larger aromatic rings, such as quinoline (**10b-01** and **10b-02**), benzofuran (**10b-03** and **10b-04**) and benzothiophene (**10b-05**), dibenzothiophene (**10b-06**), the cytotoxicity was either retained or slightly decreased (Table S**2**). Among these compounds, target compound **071**, **10b-01** and **10b-04** were selected for evaluation of their metabolic stability in human and mouse liver microsomes. The results, presented in Table S**5**, indicated that the stability of **10b-01** significantly reduced, while the stability of **10b-04** was slightly reduced compared to **071**.

Next, the N-linked phenyl group of compound **071** was replaced by more hydrophilic groups, including pyridinyl (**10c-01** and **10c-02**) and pyrazine (**10c-03**). The cytotoxicity data of these compounds are presented in Table S**3**. The results indicated that both the target compound alone and in combination with 10 μM Apatinib exhibited lower cytotoxicity compared to **071**. Among the compound **10c-01**, **10c-02** and **10c-03**, compound **10c-02**, which exhibited relatively high combination cytotoxicity, was selected for further modification. Modification included the introduction of methyl (**10c-04**), methoxyl (**10c-05**), dimethylamino (**10c-06**) and cyano (**10c-07**) group into the pyridinyl moiety. These modifications resulted in a 1- to 2-fold enhancement in cytotoxicity compared to the unsubstituted pyridinyl group. However, compared to compound **071**, the cytotoxicity of target compounds, both alone and in combination with 10 μM Apatinib, did not show improvement. The target compound **10c-02**, **10c-04** and **10c-07** were selected for assessment of their metabolic stability in human and mouse liver microsomes. The results (Table S**5**) demonstrated that replacing the phenyl group of compound **071** with a pyridinyl group (**10c-02**) resulted in a significant decrease in stability. However, the introduction of substituent groups in the pyridinyl moiety (**10c-04** and **10c-07**) improved the stability of the resulting compounds to some extent, although it remained lower than that of the phenyl-substituted compound **071**. This finding indicates that N-linked phenyl group of **071** is critical for both the activity and stability of the target compounds.

After identifying the N-linked phenyl ring as a crucial component for maintaining activity, we focused our attention on the substituents on the phenyl ring. Various substituents, including methyl, methoxyl, fluorine, trifluoromethyl, trifluoromethoxyl, amino or dimethylamine, were respectively introduced on the phenyl ring of **071**. The cytotoxicity data (Table S**4**) revealed that the attachment of electron-donating groups, such as a methyl, methoxy group and dimethylamine at the 3-position of the phenyl ring exhibited greater potency than these groups at the 2- and 4-positions of the phenyl ring (**10d-02** vs **10d-01** and **10d-03**, **10d-05** vs **10d-04** and **10d-06**, **10d-08** vs **10d-07** and **10d-09**). Conversely, the attachment of an electron-withdrawing trifluoromethyl at the 4-position of the phenyl ring showed higher potency compared to its placement at the 2- and 3-positions (**10d-20** vs **10d-18** and **10d-19**). In addition, the attachment of dimethylamine at the 3-position of the phenyl ring (**10d-08**) displayed higher cytotoxicity than attachment of amino (**10d-10**), mono-methylamine (**10d-12**) and amide (**10d-21** and **10d-22**) at the same position. Replacing the dimethylamine at the 3-position of phenyl ring of **10d-08** with diethylamine (**10d-13**) did not result in a significant improvement in cytotoxicity. We then explored the effect of disubstitution or trisubstitution (**10d-23~10d-33**) of the phenyl ring on the cytotoxicity. The results showed that these compounds had similar cytotoxicity to those with mono-substitution. Among the above compounds, **10d-02** (3-CH_3), **10d-15** (4-F) and **10d-25** (3-OCH_3, 4-CH_3) demonstrated the most potent cytotoxicity.

Next, we selected several representative compounds to evaluate their metabolic stability in human and mouse liver microsomes. The stability data (Table S**6**) demonstrated that the methyl substituents at the 3- and 4-positions (**10d-02, 10d-03**) of phenyl ring exhibited greater stability than the methyl substituent at the 2-position (**10d-01**). Among the compounds with mono-, di-, or trisubstitution at the phenyl ring, most exhibited stability comparable to or greater than that of compound **071**. However, the introduction of an amino group on the phenyl ring (**10d-10**) resulted in a significant decrease in stability compared to compound **071**. Overall, compound **10d-02** (3-CH_3), **10d-03** (4-CH_3), **10d-17** (4-CF_3) and **10d-33** (3-$N(CH_3)_2$, 4-Cl) exhibited optimal

metabolic stability. When considering their cytotoxicity, compound **10d-02** (3-CH_3) stands out as a candidate of significant interest for further study.

To explore the effect of the linker chain length between the phenyl and benzopyrazole on cytotoxicity, we synthesized three compounds: **10e-01** (n=1), **10e-02** (n=2) and **10e-03** (n=3). The cytotoxicity data are presented in Table S7. The results showed that as the linker length was increased, the cytotoxicity decreased. This suggests that a shorter linker is more favorable for maintaining cytotoxic activity.

Next, we synthesized compound **10f-01** (R/S configuration) and **10f-02** (S/R configuration), which were introduced a methyl in methylene between phenyl and benzopyrazole of **10e-01**. The configurations (R or S) of **10f-01** and **10f-02** have not been determined. The introduction of methyl resulted in an increase of cytotoxicity (Table S**8**). However, compared with compound **071**, their metabolic stability in human and mouse liver microsomes was significantly decreased (Table S**6**).

To preliminary explore the influence of C-linked aryl groups in the indazole scaffold of compound **071** on the cytotoxicity and metabolic stability, we also synthesized several compounds with different aryl instead of the p-ethoxyphenyl group of **071**. The results (Table S**9**) indicated that most of synthesized compounds remain their activity. Some compounds were selected to examine their metabolic stability in human and mouse liver microsomes. The results (Table S**10**) showed that replacing the p-ethoxyphenyl of **071** with p-methoxyphenyl (**23a**), p-isopropyphenyl (**23b**), p-methyphenyl (**23c**), p-ethyphenyl (**23d**) or p-cyclopropyphenyl (**23e**) resulted in a slight decrease in stability, particularly for p-methyphenyl (**23c**) and p-ethyphenyl (**23d**). In contrast, replacing the 4-p-ethoxyphenyl group of compound **071** with benzothienyl (**23f**) improved the stability.

Based on the aforementioned results, the target compounds **10d-02** and **23f** were selected to calculate their combination index (CI) at IC_{50} and IC_{60}. The results are

presented in Table S**11**. The CI value is crucial in defining the mode of drug interaction. A strong synergism effect (CI = 0.2-0.6) was observed for the combination of **10d-02** with Apatinib (10 μM). Moderate synergism (CI = 0.6-0.8) was observed for the combination of **23f** with Apatinib (10 μM) at IC_{50} in the same HGC-27 cell line. These findings indicate that compound **10d-02** exhibit a strong synergistic effect when combined with Apatinib, making it a promising candidate for further development in combination therapies.

Inhibition Effects of Selected Compounds on hERG Channels

Cardiac arrhythmias are a common adverse effect observed during the drug development process and are often linked to a drug's ability to inhibit the hERG cardiac potassium channel. Therefore, we evaluated the hERG inhibition potential of compounds **071**, **10d-02**. Terfenadine served as a positive control, demonstrating an inhibition rate of 26.0% at a concentration of 0.01 μM. At a concentration of 10 μM, compounds **071**, **10d-02** exhibited relatively low hERG inhibition rates of 27.7% and 27.3%, respectively, suggesting minimal cardiotoxic potential.

Broad-spectrum combination effects of compound 10d-02 with various RTK inhibitors

We next tested the combination effects of the target compound **10d-02** with Apatinib and Gefitinib against five different human tumor cell lines, as listed in Table 3. The results demonstrated that compound **10d-02** exhibited broad-spectrum combination activity with Apatinib and Gefitinib, effectively inhibiting the growth of all tested cell lines. Regardless of their sensitivity to Apatinib and Gefitinib, the combination with **10d-02** significantly reduce their IC_{50} values in these cancer cell lines. Moreover, **10d-02** also enhanced the cytotoxic effect of Sorafenib, Lenvatinib, and Regorafenib, all of which are approved VEGFR inhibitors for the treatment of hepatocellular carcinoma (HCC), on the JHH-7 cell line (Fig. **2C**). To further investigate the synergistic effect of

compound **10d-02** with Gefitinib against Gefitinib-insensitive cell line, we determined the tumor growth inhibition effect of combining **10d-02** with Gefitinib using the H1975 and A549 cell line. the combination of compound **10d-02** and Gefitinib conferred a significant synergistic effect in both H1975 and A549 cells. Compared with compound **071**, the combination of 10 μM **10d-02** reduced the IC_{50} of Gefitinib from 201 μM to 2.3 μM in H1975 cells (Fig. **2d**). 5 μM **10d-02** lowered the IC_{50} value from 12.25 μM to 3.37 μM in A549 cells (Fig. **2E**). Compared to **071**, **10d-02** exhibited a better synergistic effect in Gefitinib-insensitive cell lines. Overall, these findings indicate that compound **10d-02** has a more consistent and broad-spectrum combination activity with various RTK inhibitors across multiple human tumor cell lines than compound **71**. Therefore, compound **10d-02** was selected for further testing of its in vivo activity with multiple TKIs to evaluate its potential as a synergistic agent in combination therapies.

Table **3**. In vitro combination activity and anti-drug resistance of compound **10d-02** with Apatinib (A) and Gefitinib (G).

Cell line	Comp.	IC_{50} (μM)	Cell line	Comp.	IC_{50} (μM)
KYSE30	A	11.99	MCF-7	A	15.49
	G	12.63		G	9.70
	10d-02	4.11		10d-02	5.78
	10d-02 + A (5 μM)	0.82		10d-02 + A (5 μM)	1.91
	10d-02 + G (5 μM)	0.40		10d-02 + G (5 μM)	1.68
DU145	A	5.73	RBE	A	13.72
	G	5.85		G	20.17
	10d-02	3.06		10d-02	12.48
	10d-02 + A (3 μM)	0.07		10d-02 + A (10 μM)	1.63
	10d-02 + G (3 μM)	0.49		10d-02 + G (10 μM)	1.05
HeLa	A	54.34			
	G	6.42			
	10d-02	6.64			
	10d-02 + A (5 μM)	2.04			
	10d-02 + G (5 μM)	0.61			

Pharmacokinetic characterization of compounds 10d-02 and 071

Based on the favorable in vitro potency profiles, compounds **10d-02** was selected for further pharmacokinetic characterization compared to **071.** The results of the mouse pharmacokinetic studies for these compounds are summarized in Table **4**. Both compounds exhibited pharmacokinetic profiles characterized by a long half-life ($T_{1/2}$), high maximum concentration (Cmax), and good oral bioavailability (F). Notably, compound **10d-02** demonstrated an improved oral half-life, intravenous and oral Cmax and oral bioavailability.

Given these promising pharmacokinetic attributes, compound **10d-02** was identified as a lead candidate for subsequent mechanism and efficacy testing in xenograft models. Additionally, a fourteen-day dose range-finding study of **10d-02** in rats was conducted. No body weight loss or abnormal physical conditions were observed across the three dose groups (100, 500, and 1000 mg/kg/day), indicating that **10d-02** has a high safety profile.

Table **4**. Pharmacokinetic data of compounds **10d-02** and **071** at 5 mg/kg (iv) and 10 mg/kg (po).

	dose	N	$T_{1/2}$	C_{max}	$AUC_{(0-t)}$	$AUC_{(0-\infty)}$	CL
I.V.	mg/kg		hr	ng/mL	h*ng/mL	h*ng/mL	mL/min/kg
10d-02	5	3	1.69	3397	2462	2533	32.98
071	5	3	1.79	2448	1645	1687	50.37

	dose	N	$T_{1/2}$	C_{max}	$AUC_{(0-t)}$	$AUC_{(0-\infty)}$	F
P.O.	mg/kg		hr	ng/mL	h*ng/mL	h*ng/mL	%
10d-02	10	3	4.79	1138	5783	6924	97.4
071	10	3	3.5	1012	3043	3757	92.5

CL, clearance; N, number of animals.

In vivo synergistic effects of compound 10d-02 in combination with RTK inhibitors

To evaluate the in vivo efficacy of compound **10d-02** in combination with RTK inhibitors, we utilized a cell-derived tumor xenograft (CDX) model in nude mice. The

human gastric cancer cell line HGC-27 was subcutaneously transplanted into the armpit region of nude mice. When the average tumor volume reached approximately 100 mm^3, the mice were randomly assigned to receive daily oral gavage of either **10d-02**, Apatinib or a combination of **10d-02** with Apatinib. Two concentrations of **10d-02** were tested in combination with Apatinib. Our observations revealed that **10d-02** alone had no therapeutic effect, whereas Apatinib significantly reduced tumor growth rate compared to the control group. Notably, the combination of 90 mg/kg **10d-02** with Apatinib significantly suppressed tumor growth compared to Apatinib monotherapy (Fig. **3A**). Although there was no statistically significant difference in the combination of 45mg/kg **10d-02**, it also showed a trend of increased efficacy (Fig. **3A**). The addition of **10d-02** to Apatinib did not result in increased weight loss compared to Apatinib monotherapy, indicating no significant additional toxicity (Fig. **3B**). Furthermore, to confirm that the enhancing efficacy of **10d-02** is applicable to various VEGFR inhibitors, we investigated the combination effect of **10d-02** with Lenvatinib in the mice bearing HCC cell line Hep3B and colon cancer cell line HCT116 xenograft. The results showed that single treatment with **10d-02** hardly caused tumor growth inhibition compared to the control. However, the combination of **10d-02** with Lenvatinib exhibited a more potent tumor growth inhibition effect than Lenvatinib alone (Fig. **3C and 3E**). Importantly, no obvious body weight loss or abnormal physical conditions were observed during the treatment (Fig. **3D and 3F**). The combined anti-tumor effect of **10d-02** is also applicable to another VEGFR inhibitor, Axitinib (Fig. **3G and 3H**).

Given that the third-generation EGFR inhibitor, Osimertinib, is currently the first-line therapy for non-small cell lung cancer and our cell experiments showed that compound **071** could improve the activity of Osimertinib, we explored whether **10d-02** could enhance the efficacy of Osimertinib in vivo. Using the H1975 cell line, which is sensitive to Osimertinib, we established a subcutaneous transplant tumor model in nude mice. When the average tumor size is 200mm^3, Osimertinib and **10d-02** were administered by gavage, either alone or in combination. The results showed that 2.5 mg/kg Osimertinib monotherapy rapidly reduce tumor mass, lasting for about one week, after which the tumor ceased to shrink. However, tumor volume continued to decline

in the combination group (Fig. **3I**). There was no significant difference in weight change between the combination therapy group and the monotherapy group (Fig. **3J**). Due to the combination group was still effective even after a certain degree of tolerance to Osimertinib monotherapy, we attempted to further investigate the potential of **10d-02** in prolonging the effective duration of Osimertinib treatment. We performed an administration of orally 2.5mg/kg of Osimertinib alone once a day on H1975 xenograft model when the average tumor volume reached 200 mm^3. After one week, when the tumor volume began to increase again, the dosage was adjusted to 5 mg/kg until the tumors adapted and the average volume grew to 400 mm^3. Subsequently, **10d-02** was administered orally at 90 mg/kg in combination with 5 mg/kg Osimertinib once daily. The results demonstrated that the addition of **10d-02** restored the therapeutic effect of Osimertinib once again (Fig. **3K**), The decrease in the curve of the Osimertinib group was attributed to the euthanasia of mice with excessively large or damaged tumors. Body weight and physical observations indicated that the combination of **10d-02** and Osimertinib was well tolerated during treatment (Fig. **3L**). These findings suggest that compound **10d-02**, when used in combination with RTK inhibitors such as Apatinib, Lenvatinib, and Osimertinib, can significantly enhance anti-tumor efficacy without increasing toxicity, thereby offering a promising therapeutic strategy for cancer treatment.

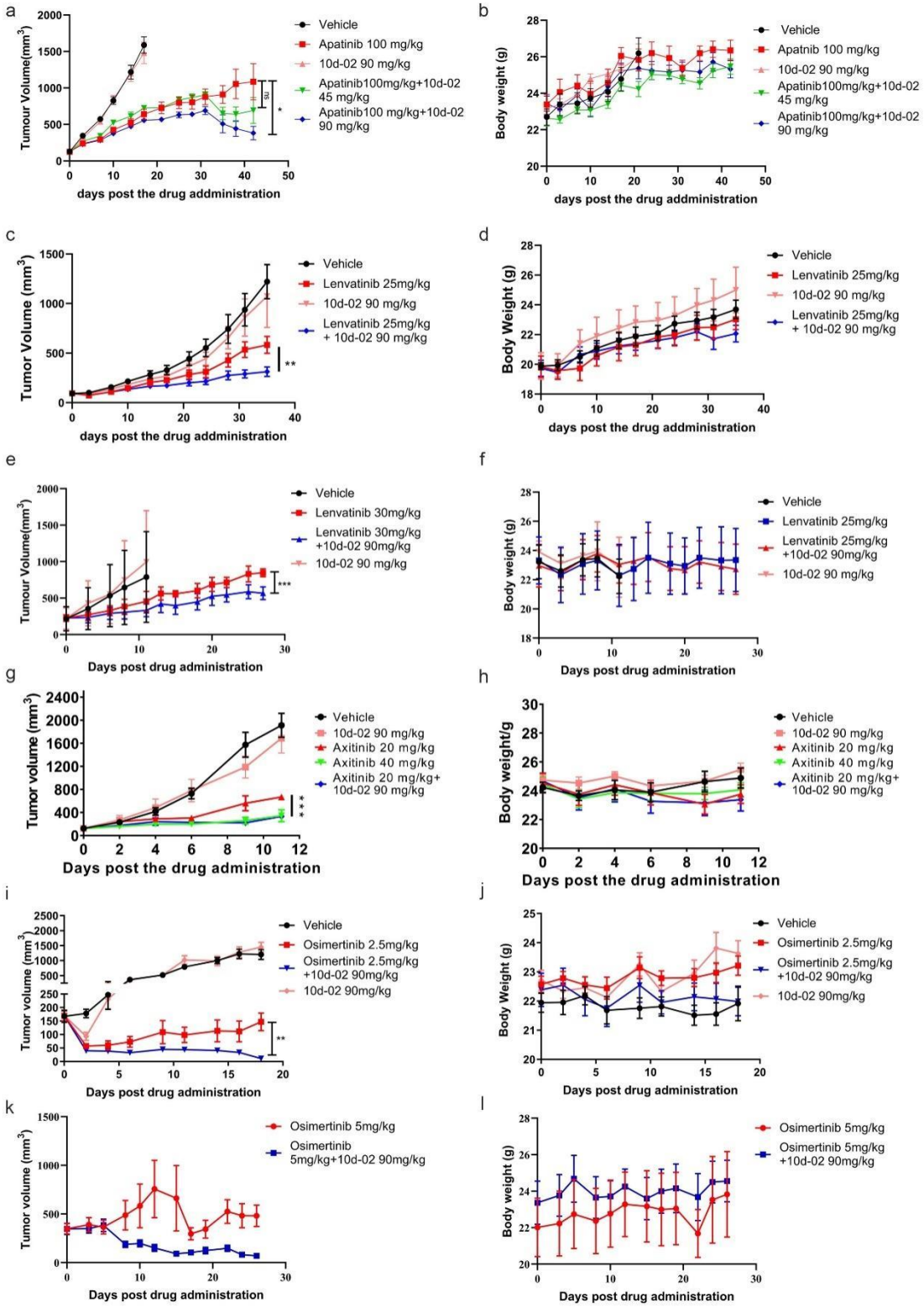

Figure **3**. In vivo antitumor efficacy of Apatinib, Lenvatinib, Axitinib and Osimertinib or their combination with compound **10d-02**. Mice bearing xenografts of the human gastric cancer cell line HGC-27 were gave indicated doses of Apatinib (A and B). Mice bearing xenografts of the human HCC cell line Hep3B or colon cancer cell line HCT116

were gave indicated doses of Lenvatinib (C-F) alone or along with compound **10d-02** when tumors reached 100–200 mm^3. Mice bearing xenografts of the human HCC cell line JHH-7 were gave indicated doses of Axitinib (G and H) alone or along with compound **10d-02** when tumors reached 100–200 mm^3. (A-H) Tumor volumes and body weights were measured twice a week and plotted the curve using mean±SEM (n=6). (I-L) 5×10^6 Human NSCLC cell line H1975 were inoculated subcutaneously and were treated with 2.5 mg/kg Osimertinib alone or simultaneously administered with 90 mg/kg compound **10d-02** (I and J). For K and L, the tumor bearing mice were given compound **10d-02** when the tumor tolerating a dose of 5 mg/kg Osimertinib and reached to 400 mm^3. Tumor volumes and body weights were calculated twice a week and plotted the curve using mean±SEM (n=6). Student *t*-test is used to statistically analyze tumor volumes with significant differences. * $p<0.05$, ** $p<0.01$ and *** $p<0.005$.

Mechanistic insights into the synergistic effects of compound 10d-02 and RTK inhibitors.

To elucidate the mechanisms underlying the enhanced activity of receptor tyrosine kinase (RTK) inhibitors when combined with the derivatives of compound **071**, we investigated the effects of compound **10d-02** on the expression of key RTKs. Our findings revealed that **10d-02** significantly reduced the protein levels of EGFR T790M (an Osimertinib-sensitive mutation), VEGFR2, and VEGFR3 (Fig. 4A and 4B). When cells were treated with a combination of **10d-02** and inhibitors of targeting EGFR, VEGFR2, or VEGFR3, the protein levels of these RTKs were further reduced compared to treatment with the corresponding RTK inhibitors alone (Fig. 4A and 4B). This suggests that compound **10d-02** synergistically enhances the degradation of these RTKs, thereby potentiating the efficacy of the RTK inhibitors.

To investigate the mechanism by which the combination of **10d-02** and TKIs leads to RTK degradation, we identified potential cellular targets of **10d-02**. Using established

methods for identifying small molecule binding proteins[18], we chemically modified **10d-02**. We prepared **DA-10d-02** by introducing a bifunctional side chain containing diazirine and alkyne (Fig. 4C). Diazirine was used for photoaffinity labeling of target proteins in situ by forming covalent bonds, while the alkyne was conjugated with the reporter biotin-PEG-azide or 5-TAMRA-azide via a click reaction.

DA-10d-02 exhibited similar cellular activity and the ability to degrade VEGFR3 in combination with Lenvatinib to **10d-02**, indicating that the introduction of modifying groups did not affect the chemical properties of **10d-02** (Fig. 4D and 4E). Next, we conducted in-gel fluorescence analysis to determine the protein labeling capacity of **DA-10d-02**. HEK293T cells were incubated with **DA-10d-02** and exposed to UV irradiation. The cell lysates were then conjugated to 5-TAMRA-azide via click reaction. In-gel fluorescence scanning showed that the fluorescence intensity of labeled proteins was significantly reduced in the presence of an excess amount of **10d-02** for competition (Fig. 4f) indicating that **DA-10d-02** can be used to capture protein targets in cells. Subsequently, HEK293T cells were treated with **DA-10d-02** in the presence or absence of **10d-02**. After UV irradiation, cell lysates were prepared and biotin-PEG-azide was conjugated to **DA-10d-02** via a click reaction. The **DA-10d-02**-captured proteins were then pulled down using streptavidin beads for liquid chromatography-tandem mass spectrometry (LC-MS/MS) analysis. Mass spectrometry analysis identified a series of proteins, among which SGLT1 caught our attention (Fig. 4G). Representative SGLT1 peptide spectra are shown in Fig. 4H. Pulldown coupled with western blot analysis using **DA-10d-02** also demonstrated the interaction between **DA-10d-02** and SGLT1. This interaction could be blocked by **10d-02**, further confirming that **10d-02** targets SGLT1 (Fig. 4I).

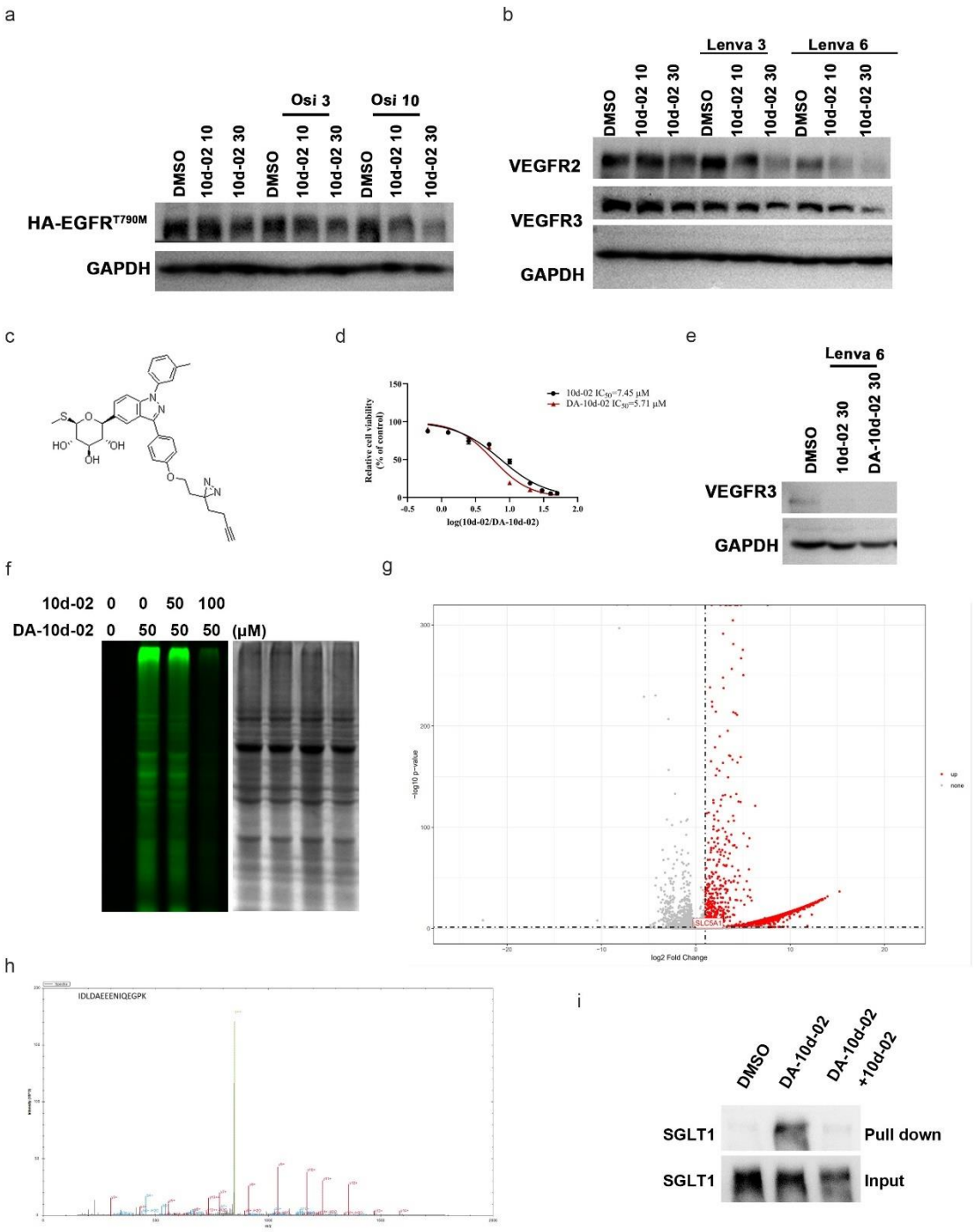

Figure 4. Expression analysis of VEGFR2/3 in JHH-7 cells and plasmids featuring EGFR T790M in HEK 293T cells after treatment with compound **10d-02** alone or in combination with variable concentrations of Osimertinib (Osi) (A) and Lenvatinib (B). Commercial HA and VEGFR2/3 antibody were utilized as the primary antibody. GAPDH was used as the loading control. (C) The chemical structure of **DA-10d-02**. (D) Survival curves of HGC-27 cells treated with varying concentrations of **10d-02** or **DA-10d-02**. (E) Western blot assay VEGFR3 protein level in JHH-7 cells treated with

10d-02 or **DA-10d-02** in combination with Lenvatinib. (F) In situ fluorescence labeling of HEK293T cells treated with 50 μM **DA-10d-02**. For the competition assay, HEK293T cells were pretreated with different concentrations of **10d-02** for 1 h, and then co-treated with **DA-10d-02** for 3h. (G) Volcano plot of the targets identiffed by LC–MS/MS analysis. Red blots indicated signiffcant targets with fold change greater than 2 and p value less than 0.05. These experiments were performed in triplicate for each group. (H) Representative LC–MS/MS site-mapping data showing the interaction between SGLT1 and **DA-10d-02**. (I) SGLT1 were pulled down from HEK293T by **DA-10d-02** in immunoblot assay. SGLT1 pulled down by **DA-10d-02** were competitively inhibited by **10d-02**.

SGLT1 interacts with VEGFR2/3 and prolongs their half-life

Previous studies have shown that SGLT1 binds to EGFR[19]; however, it is unclear whether SGLT1 also interacts with VEGFR2/3. To investigate this, we constructed expression vectors for SGLT1 and VEGFR2/3 and performed co-immunoprecipitation analysis after co-transfecting 293T cells. The results demonstrated that SGLT1 can bind to VEGFR2/3 (Fig. 5A and 5B). Additionally, immunoprecipitation experiments using an SGLT1 antibody in the JHH-7 cell line further confirmed the interaction between SGLT1 and VEGFR2/3 (Fig. 5C and 5D).

Next, we examined whether SGLT1 could increase the stability of VEGFR2/3. We used cycloheximide (CHX) to inhibit protein translation and observed the half-life of VEGFR2/3 in the presence of SGLT1(Fig. 5E and 5F). The results showed that SGLT1 increased the expression levels of VEGFR2/3 and extended their half-life. These findings indicate that SGLT1 not only binds to EGFR but also acts as a stabilizing partner for VEGFR2/3, thereby expanding the functional role of SGLT1. We developed SGLT1 knockdown cell lines and assessed the expression levels of VEGFR2 and VEGFR3. Our findings revealed a decrease in the protein levels of VEGFR2 and VEGFR3, aligning with the increased sensitivity of the SGLT1

knockdown cell line to VEGFR inhibitors (Fig. 5G and 5H).

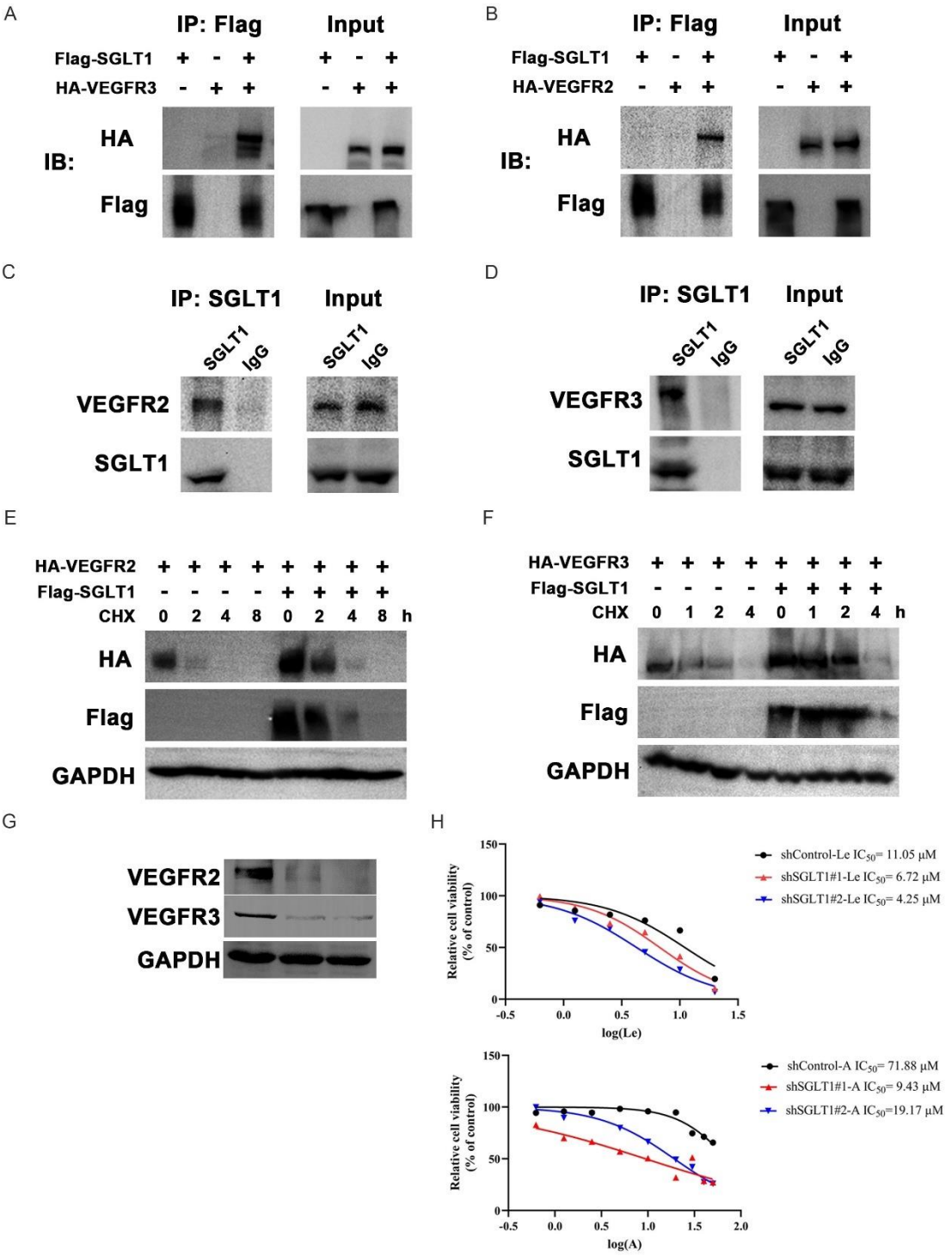

Figure 6. Validation of the Interaction Between SGLT1 and VEGFR2/3.

(A and B), HEK293T cells were co-transfected with Flag-tagged SGLT1 and HA-tagged VEGFR2/3. After 24 hours, cells were harvested and lysed with RIPA buffer. Lysates were prepared for pull-down analysis using Flag-affinity magnetic beads. (C and D), the HCC cell line JHH-7 was lysed and subjected to immunoprecipitation analysis using an SGLT1 antibody or control IgG. The presence of VEGFR2/3 in the immunoprecipitates was detected by Western blot using VEGFR2/3 antibodies.
(E and F), HEK293T cells were co-transfected with Flag-tagged SGLT1 and HA-tagged VEGFR2/3. After 12 hours, cells were treated with 200 μg/mL cycloheximide (CHX). Cells were harvested at different time points post-treatment, and VEGFR2/3 protein levels were analyzed by Western blot. (G) Expression analysis of VEGFR2/3 in wild-type or SGLT1-knockdown JHH-7 cells. Commercial HA and VEGFR2/3 antibody were utilized as the primary antibody. GAPDH was used as the loading control. (H) Survival curves of wild-type or SGLT1-knockdown JHH-7 cells treated with varying concentrations of Lenvatinib(Le) and Apatinib(A).

Compound 10d-02 disrupts the interaction between SGLT1 and RTKs

Given that SGLT1 is known to bind RTKs, we investigated whether **10d-02** could interfere with this interaction. HEK293T cells were co-transfected with expression plasmids for SGLT1 and RTKs. Subsequently, the cells were treated with **10d-02** for 4 hours. The treated cells were then subjected to immunoprecipitation analysis. Consistent with previous studies, our results confirmed that SGLT1 interacts with EGFR, and this interaction can be disrupted by **10d-02** (Fig. 6A). Similarly, **10d-02** was also able to block the interaction between SGLT1 and VEGFR2/3 (Fig. 6B and 6C). Previous studies have demonstrated that the interaction between EGFR and SGLT1 plays a crucial role in stabilizing SGLT1[19]. Given that 10d-02 disrupts this interaction, it is likely to result in a reduction of SGLT1 protein. Upon testing, we observed that treatment with 10d-02 indeed led to a decrease in SGLT1 protein levels (Fig. 6D). Since SGLT1 stabilized VEGFR2 and VEGFR3, this finding also provides an explanation for why 10d-02 can reduce the levels of VEGFR2 and VEGFR3. These results provide valuable mechanistic insights into how compound **10d-02** enhances the activity of RTK

inhibitors, indicating its potential as a promising agent in combination therapies targeting drug-resistant tumor types (Fig. 6E).

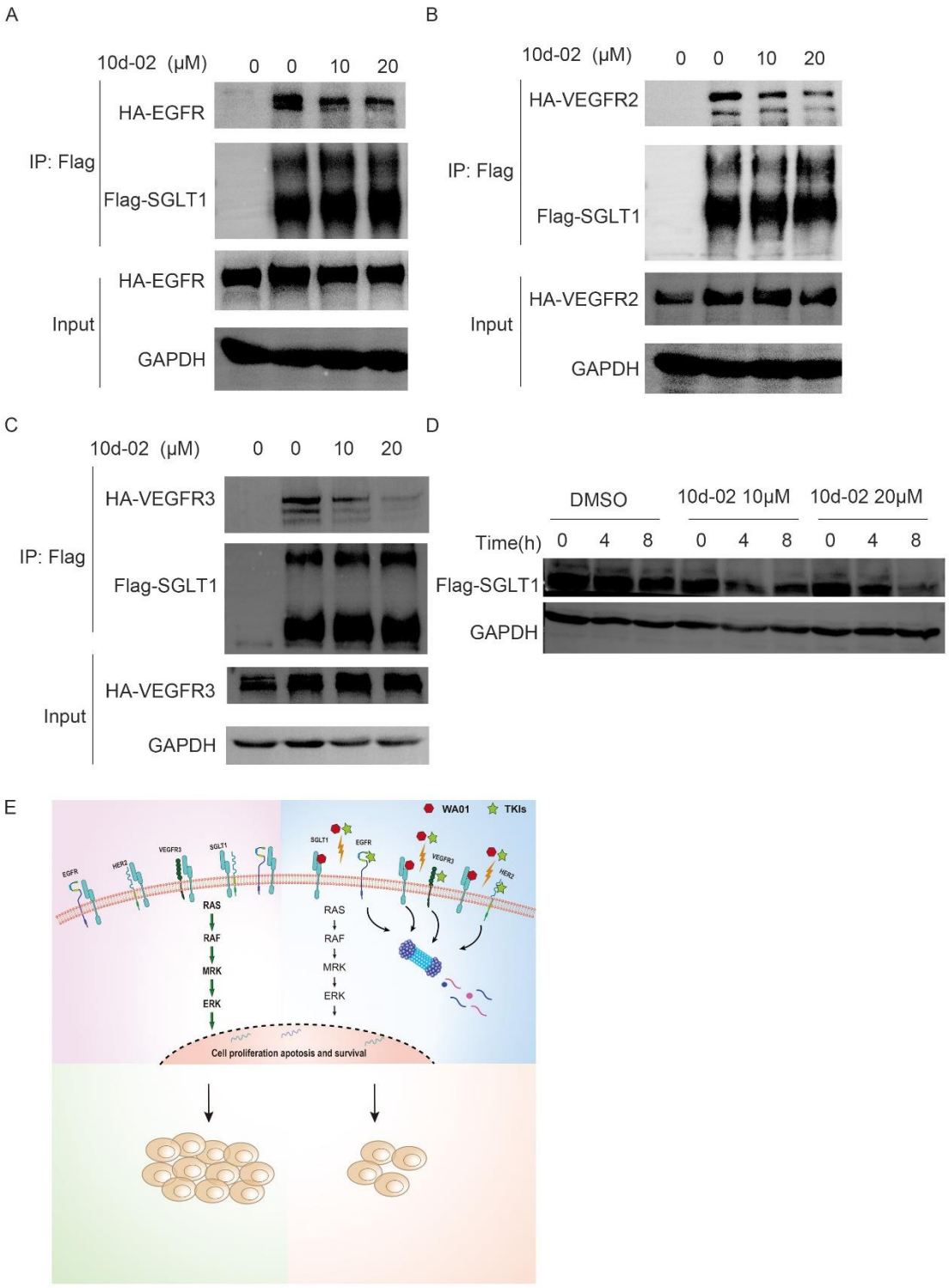

Figure 6. 10d-02 inhibits the interaction between SGLT1 and RTKs

HEK293T cells were seeded in a 10 cm dish. (A-C), When the cells reached

approximately 70% confluence, they were co-transfected with 5 μg of Flag-tagged SGLT1 plasmid and 10 μg of HA-tagged VEGFR2/3 or EGFR plasmid. After 20h transfection, the cells were treated with varying concentrations of **10d-02** or DMSO for 4 hours. Following treatment, the cells were harvested for immunoprecipitation analysis. The presence of VEGFR2/3 or EGFR was detected using a HA antibody, while Flag antibody was used to detect SGLT1. (D) Expression analysis of SGLT1 in 10d-02 treated cells. (E) Schematic diagram illustrating the mechanism by which compound 10d-02 targets SGLT1 to enhance the efficacy of TKI therapy.

Conclusion

In this study, we report the identification of a novel compound, designated **071**, which characterizes an indazole core surrounded by a carbohydrate moiety and two phenyl groups. This compound demonstrated synergy with various receptor tyrosine kinase (RTK) inhibitors, thereby enhancing their antitumor activity. To investigate the structure-activity relationship and optimize the synergistic effect, we modified the structure of compound **071**, leading to the synthesis and evaluation of several analogues for their synergistic antitumor effects and metabolic stability. Among these analogues, compound **10d-02** was identified as notably superior, exhibiting enhanced antitumor activity and stability compared to the parent compound **071**. Notably, **10d-02** displayed a favorable pharmacokinetic (PK) profile, achieving an oral bioavailability of approximately 100%. In vivo, the combination of **10d-02** with Apatinib, Axitinib or Lenvatinib showed significantly greater efficacy than treatment with either RTK inhibitor alone. Moreover, combining **10d-02** with Osimertinib enhanced antitumor efficacy in both Osimertinib-sensitive and -insensitive tumor xenograft models, without evident toxicity. Furthermore, the combination of 10d-02 and regorafenib did not exhibit any significant new or synergistic toxic reactions in either rat or dog studies. Consequently, non-clinical toxicology studies indicate that the use of 10d-02 in combination with the TKI regorafenib demonstrates a favorable safety profile. In conclusion, compound **10d-02** and its analogues represent promising candidates for

combination therapy with RTK inhibitors in cancer treatment. Efforts to further elucidate the clinical potential of **10d-02** and its analogues are currently underway.

Using click chemistry and mass spectrometry analysis, we identified a series of potential target proteins for **10d-02**. Among these, we prioritized the validation of SGLT1, as it was previously shown to interact with and stabilize EGFR[19]. In our study, we further discovered that SGLT1 can also interact with and stabilize VEGFR2/3. This suggests that SGLT1 may broadly bind to various RTKs, potentially serving as a general chaperone protein for RTKs. This finding also reveals an additional function of SGLT1 beyond its role in glucose transport. High expression of SGLT1 has been associated with poor prognosis in various cancers[20]. In some of these cancers, the poor prognosis cannot be solely explained by the interaction between SGLT1 and EGFR. Our findings may provide further insights into the role of SGLT1 in cancer progression.

Understanding the exact molecular interactions and pathways involved will provide deeper insights into the synergistic effects observed and could lead to the development of more effective combination therapies. By pinpointing the specific targets and mechanisms of action, we aim to optimize the therapeutic potential of compound **10d-02** and related derivatives, ultimately improving treatment outcomes for patients with drug-resistant tumors.

Experimental section

Chemistry

This secction can be found in supplementary information.

Cytotoxicity Assay.

The cells (HGC-27, cat. CTCC-002-0006, H1975, cat. CTCC-001-0354, A549, cat. CTCC-001-0036, JHH-7, cat. CTCC-004-0053, HEK293T, cat. CTCC-001-0188, KYSE30, cat. CTCC-400-0150, MCF-7, cat. CTCC-001-0042, DU145, cat. CTCC-001-0013, RBE, cat. CTCC-003-0101, and HeLa, cat. CTCC-001-0006) were purchased from Zhejiang Meisen Cell Technology Co., Ltd. The cells were cultured in DMEM or RPMI 1640 medium supplemented with 10% fetal bovine serum (FBS) at 37°C in 5% CO_2. Cells were plated in 96-well plates at a density of 3000-5000 cells per well. After overnight, cells were incubated with serial dilutions of target compounds or DMSO for 48 h. The cell growth was evaluated with Thiazolylblue tetrazolium bromide (MTT) Assay (Solarbio, cat. M8180) according to the manufacturer's instruction. All tested compounds are >95% pure by HPLC (Waters ACQUITY UPLC I-CLASS PLUS/XEVO G3 QTOF (UPLC-Q-TOF-MS)) analysis.

Metabolic Stability Studies

The mouse liver microsome was purchased from Xenotech. The human liver microsome was purchased from BioreclamationIVT. Metabolic stabilities of the test compounds in mouse and human liver microsomes were determined at 1 μM. The compounds were incubated with 0.5 mg protein/mL in phosphate buffer at 37°C. The reaction was started with the addition of 1 mM NADPH. The incubation solution was incubated in water batch at 37°C. At 0, 5, 15, 30 and 60 minutes, the reaction was stopped by the addition of the cold MeOH: acetonitrile=1:1 with IS (50 ng/mL Labetalol, 50 ng/mL Tolbutamide). Samples were centrifuged at 4000 rpm for 10 minutes. The supernatants were analyzed by LC-MS/MS (Shimadzu 2020-ELSD).

Pharmacokinetic Studies

ICR mice were orally (PO, 10 mg/kg) or intravenously (IV, 5 mg/kg) administered with test compounds. The test compounds were dissolved in 5% DMSO/30% PEG300/10% Tween 80/55% H_2O. Blood was collected from the facial vein at 5 min, 15 min, 30 min, 1 h, 2 h, 4 h, 6 h, 8 h, 24 h after administration. The plasma concentrations of test compounds were determined by LC-MS/MS (Shimadzu 2020-ELSD).

Fourteen-day dose range-finding studies

The dose range-finding study was conducted to determine the the toxicologic effects of **10d-02** when administered to rats for 14 days. The **10d-02** was suspended in an aqueous solution containing 1% HPMC (hydroxypropyl methyl cellulose) and administered orally (gavage) at dosages of 0, 100, 500, or 1000 mg/kg/day daily for 14 days. The body weight and physical condition were monitored.

hERG assay

When the fusion of HEK-293-hERG (Human Embryonic Kidney cells stably expressing hERG potassium channels) reached over 75% confluence, the cells were dissociated and re-suspended in culture medium. After centrifugation, the supernatant was discarded, and the cells were re-suspended in an extracellular solution, and stored in a tube at 2-8 ℃. Prior to recording, cells will be seeded into 35 mm culture dish at a density with single disparately state. Compound or Positive control will be tested at room temperature using the whole-cell patch clamp techniques with a PatchMaster patch-clamp system (HEKA Elektronik, Germany), following the manufacturer's instruction.

In vivo efficacy assessment

Eight-week-old male Balb/c nude mice were purchased from Charles River Laboratories Co., Ltd. and raised at Peking Union-Genius Pharmaceutical Technology Company (Beijing, China). The entire experimental process received approval and supervision from the Peking Union-Genius Institutional Animal Care and Use Committees (IACUC). The ethic number is JY24005. Mice were injected

subcutaneously with 5×10^6 HGC-27, HCT116, JHH-7, Hep3B or H1975 cells per mouse. When the average tumor volume reached 200-400 mm^3, the mice were randomly distributed into vehicle, compound **10d-02** (45 mg/kg and 90mg/kg), Apatinib, Lenvatinib, Axitinib or Osimertinib alone and their combination. Treatments were administered orally once a day. Subcutaneous tumors were measured every two days or two times a week. Tumor volume was calculated using the formula $(L\times W^2)/2$. When the tumor volume exceeds 2000 mm^3 or decays, mice will be euthanized using carbon dioxide anesthesia.

The ABPP-based target exploration

HEK293T cells were cultured and incubated with **DA-10d-02** for 4 h. After removing the culture medium, the plates were exposed to UV lamps for 30 min. Then, cells were harvested and lysed in PBS buffer containing 1% SDS by sonication (25 % amplification, 2 s on and 2 s off for 2 min). Protein was mixed with 0.2 mM azide-TAMRA (MCE, cat. HY-151857), 0.1 mM TBTA (MCE, cat. HY-116677) and 1.0 mM TCEP (MCE, cat. HY-W011500). Samples were gently vortexed and 1.0 mM $CuSO_4$ was added to initiate the click reaction. The reaction was incubated at 37 ˚C for 2 h in an incubator shaker (300 rpm). Then the labeled proteins were precipitated with prechilled acetone and washed with ice-cold methanol twice. For fluorescence detection, the samples were dissolved with 1×SDS loading buffer and boiled at 95 °C for 10 min, and then separated by 10% SDS-PAGE gel. The fluorescence gels were detected by gel imager (Protein Simple, FluorChem M) and protein loading visualized with coomassie blue staining.

For LC-MS/MS and immunoblot detection, HEK293T cells were pretreated with **10d-02** or DMSO for 1 h and then treated with **DA-10d-02** for 3h. After being exposed to UV lamps and lysed, the protein samples were combined with the pre-mixtures of 0.1 mM biotin-PEG3-azide (MCE, cat. HY-130143), 0.1 mM TBTA and 1.0 mM TCEP. Then, 1.0 mM $CuSO_4$ was added. The mixtures were incubated at 37 ˚C for 2 h in an incubator shaker (300 rpm). After the proteins being precipitated and washed, samples

were dissolved in PBS buffer with 1.2% SDS, and incubated with washed Pierce Streptavidin Magnetic Beads for 3h at room temperature. The proteins captured on streptavidin beads were digested to peptides with trypsin. These peptides were analyzed by LC-MS/MS. For immunoblot, the beads were washed three times with TBS-T buffer and mixed with 1 × loading buffer, followed by boiling at 95 °C for 10 min, then detected by immunoblot analysis.

Western Blot

HGC-27 cells or HEK293T cells transfected with HA-tagged EGFR or VEGFR3 for 24 hours were treated with compound **10d-02** alone or in combination with Osimertinib (MCE, cat. HY-15772), Lapatinib (MCE, cat. HY-50898), Lenvatinib (MCE, cat. HY-10981) at the indicated concentrations for 18 hours and then lysed with RIPA buffer (50 mM Tris-HCl, pH 8.0, 150 mM NaCl, 1.5 mM MgCl2, 0.1% SDS, 0.5% deoxycholate (DOC), 1% NP-40) added with protease and phosphatase inhibitors (Roche). Then, western blot analysis of proteins from different lysates was performed. Briefly, protein samples were resolved by 10% SDS-PAGE gel electrophoresis and transferred onto a PVDF membrane. After blocking membranes with selected antibodies, proteins were detected with Clarity Western ECL Substrate using the ChemiDoc. The following antibodies were used for immune-blot analysis: anti-HA (Biodragon, cat. B1003), anti-VEGFR2 (CST, cat. 4290S), anti-GAPDH (Biodragon, cat. B1034).

Statistical analysis

Statistical analysis was performed using GraphPad Prism 5 (GraphPad Software Inc.). Student t-test is used to statistically analyze the significant differences. * $p<0.05$, ** $p<0.01$ and *** $p<0.005$.

Disclosure of Conflicts of Interest

None of the authors have competing financial interests to declare.

Acknowledgements

We thank Beijing Nova Program (20230484313) and Newish Biological R&D Center (Newish Biotechnology Co., Ltd.) for funding to support this study. We also appreciate the chemical synthesis services provided by Shanghai Medicilon Biopharmaceutical Co., Ltd.

Abbreviations used

RTK, receptor tyrosine kinase; EGFR, epidermal growth factor receptor; VEGFR, vascular endothelial growth factor receptor; IGF1R, insulin-like growth factor receptor; FGFR, fibroblast growth factor receptor; STAT, signal transducer and activator of transcription; DMA, dimethylacetamide; BzCl, benzyl carbonochloridate; TBSCl, tert-butylchlorodimethylsilane; py, pyridine; DMAP, dimethylaminopyridine; NBS, N-bromosuccinimide.

References

1 Bhullar KS, Lagarón NO, McGowan EM, Parmar I, Jha A, Hubbard BP, et al. Kinase-targeted cancer therapies: progress, challenges and future directions. *Molecular cancer* 2018;**17**.

2 Voldborg BR, Damstrup L, Spang-Thomsen M, Poulsen HS. Epidermal growth factor receptor (EGFR) and EGFR mutations, function and possible role in clinical trials. *Ann Oncol* 1997;**8**:1197-206.

3 Liu Y, Li Y, Wang YX, Lin CC, Zhang D, Chen JC, et al. Recent progress on vascular endothelial growth factor receptor inhibitors with dual targeting capabilities for tumor therapy. *J Hematol Oncol* 2022;**15**.

4 Pollak M. The insulin and insulin-like growth factor receptor family in neoplasia: an update. *Nature Reviews Cancer* 2012;**12**:159-69.

5 Chen LF, Zhang YM, Yin LN, Cai BH, Huang P, Li XK, et al. Fibroblast growth factor receptor fusions in cancer: opportunities and challenges. *J Exp Clin Canc Res* 2021;**40**.

6 Montor WR, Salas AROSE, de Melo FHM. Receptor tyrosine kinases and downstream pathways as druggable targets for cancer treatment: the current arsenal of inhibitors. *Molecular cancer* 2018;**17**.

7 Roskoski RJr. Small molecule inhibitors targeting the EGFR/ErbB family of protein-tyrosine kinases in human cancers. *Pharmacological research* 2019;**139**:395-411.

8 Remon J, Steuer CE, Ramalingam SS, Felip E. Osimertinib and other third-generation EGFR TKI in

-mutant NSCLC patients. *Ann Oncol* 2018;**29**:I20-I7.

9 Hicklin DJ, Ellis LM. Role of the vascular endothelial growth factor pathway in tumor growth and angiogenesis. *J Clin Oncol* 2005;**23**:1011-27.

10 Scott LJ. Apatinib: A Review in Advanced Gastric Cancer and Other Advanced Cancers (vol 78, pg 747, 2018). *Drugs* 2018;**78**:759-.

11 Dong RF, Zhu ML, Liu MM, Xu YT, Yuan LL, Bian J, et al. EGFR mutation mediates resistance to EGFR tyrosine kinase inhibitors in NSCLC: From molecular mechanisms to clinical research. *Pharmacol Res* 2021;**167**:105583.

12 Fu K, Xie F, Wang F, Fu L. Therapeutic strategies for EGFR-mutated non-small cell lung cancer patients with osimertinib resistance. *J Hematol Oncol* 2022;**15**:173.

13 Ruan RW, Li L, Li X, Huang CY, Zhang ZM, Zhong HG, et al. Unleashing the potential of combining FGFR inhibitor and immune checkpoint blockade for FGF/FGFR signaling in tumor microenvironment. *Molecular cancer* 2023;**22**.

14 Tong CWS, Wu WKK, Loong HHF, Cho WCS, To KKW. Drug combination approach to overcome resistance to EGFR tyrosine kinase inhibitors in lung cancer. *Cancer letters* 2017;**405**:100-10.

15 Facchinetti F, Hollebecque A, Braye F, Vasseur D, Pradat Y, Bahleda R, et al. Resistance to Selective FGFR Inhibitors in

Driven Urothelial Cancer. *Cancer Discov* 2023;**13**:1998-2011.

16 Hartmaier RJ, Markovets AA, Ahn MJ, Sequist LV, Han JY, Cho BC, et al. Osimertinib plus Savolitinib to Overcome Acquired MET-Mediated Resistance in Epidermal Growth Factor Receptor-Mutated,

-Amplified Non-Small Cell Lung Cancer: TATTON. *Cancer Discov* 2023;**13**:98-113.

17 Yi M, Jiao DC, Qin S, Chu Q, Wu KM, Li AP. Synergistic effect of immune checkpoint blockade and anti-angiogenesis in cancer treatment. *Molecular cancer* 2019;**18**.

18 Huang S, Wang FJ, Lin H, Liu T, Zhao CX, Chen LG. Affinity-based protein profiling to reveal targets of puerarin involved in its protective effect on cardiomyocytes. *Biomed Pharmacother* 2021;**134**:111160.

19 Weihua Z, Tsan R, Huang WC, Wu Q, Chiu CH, Fidler IJ, et al. Survival of cancer cells is maintained by EGFR independent of its kinase activity. *Cancer Cell* 2008;**13**:385-93.

20 Koepsell H. The Na(+)-D-glucose cotransporters SGLT1 and SGLT2 are targets for the treatment of diabetes and cancer. *Pharmacol Ther* 2017;**170**:148-65.